First measurement of $\Gamma(D^{*+})$ and precision measurement of $m_{D*+} - m_{D^0}$

A. Anastassov, E. Eckhart, K. K. Gan, C. Gwon, T. Hart, K. Honscheid, D. Hufnagel, H. Kagan, R. Kass, T. K. Pedlar, J. B. Thayer, E. von Toerne, and M. M. Zoeller
Ohio State University, Columbus, Ohio 43210

S. J. Richichi, H. Severini, P. Skubic, and A. Undrus
University of Oklahoma, Norman, Oklahoma 73019

V. Savinov
University of Pittsburgh, Pittsburgh, Pennsylvania 15260

S. Chen, J. W. Hinson, J. Lee, D. H. Miller, E. I. Shibata, I. P. J. Shipsey, and V. Pavlunin
Purdue University, West Lafayette, Indiana 47907

D. Cronin-Hennessy, A. L. Lyon, W. Park, and E. H. Thorndike
University of Rochester, Rochester, New York 14627

T. E. Coan, Y. S. Gao, Y. Maravin, I. Narsky, R. Stroynowski, J. Ye, and T. Wlodek
Southern Methodist University, Dallas, Texas 75275

M. Artuso, K. Benslama, C. Boulahouache, K. Bukin, E. Dambasuren, G. Majumder, R. Mountain, T. Skwarnicki, S. Stone, J. C. Wang, and A. Wolf
Syracuse University, Syracuse, New York 13244

S. Kopp and M. Kostin
University of Texas, Austin, Texas 78712

A. H. Mahmood
University of Texas–Pan American, Edinburg, Texas 78539

S. E. Csorna, I. Danko, V. Jain,* K. W. McLean, and Z. Xu
Vanderbilt University, Nashville, Tennessee 37235

R. Godang
Virginia Polytechnic Institute and State University, Blacksburg, Virginia 24061

G. Bonvicini, D. Cinabro, M. Dubrovin, and S. McGee
Wayne State University, Detroit, Michigan 48202

A. Bornheim, E. Lipeles, S. P. Pappas, A. Shapiro, W. M. Sun, and A. J. Weinstein
California Institute of Technology, Pasadena, California 91125

D. E. Jaffe, R. Mahapatra, G. Masek, and H. P. Paar
University of California, San Diego, La Jolla, California 92093

A. Eppich, T. S. Hill, R. J. Morrison, and H. N. Nelson
University of California, Santa Barbara, California 93106

R. A. Briere, G. P. Chen, T. Ferguson, and H. Vogel
Carnegie Mellon University, Pittsburgh, Pennsylvania 15213

J. P. Alexander, C. Bebek, B. E. Berger, K. Berkelman, F. Blanc, V. Boisvert, D. G. Cassel, P. S. Drell, J. E. Duboscq, K. M. Ecklund, R. Ehrlich, P. Gaidarev, L. Gibbons, B. Gittelman, S. W. Gray, D. L. Hartill, B. K. Heltsley, L. Hsu, C. D. Jones, J. Kandaswamy, D. L. Kreinick, M. Lohner, A. Magerkurth, H. Mahlke-Krüger, T. O. Meyer, N. B. Mistry, E. Nordberg, M. Palmer, J. R. Patterson, D. Peterson, D. Riley, A. Romano, H. Schwarthoff, J. G. Thayer, D. Urner, B. Valant-Spaight, G. Viehhauser, and A. Warburton
Cornell University, Ithaca, New York 14853

P. Avery, C. Prescott, A. I. Rubiera, H. Stoeck, and J. Yelton

65 032003-1

University of Florida, Gainesville, Florida 32611

G. Brandenburg, A. Ershov, D. Y.-J. Kim, and R. Wilson
Harvard University, Cambridge, Massachusetts 02138

B. I. Eisenstein, J. Ernst, G. E. Gladding, G. D. Gollin, R. M. Hans, E. Johnson, I. Karliner, M. A. Marsh, C. Plager,
C. Sedlack, M. Selen, J. J. Thaler, and J. Williams
University of Illinois, Urbana-Champaign, Illinois 61801

K. W. Edwards
Carleton University, Ottawa, Ontario, Canada K1S 5B6
and the Institute of Particle Physics, Canada

A. J. Sadoff
Ithaca College, Ithaca, New York 14850

R. Ammar, A. Bean, D. Besson, and X. Zhao
University of Kansas, Lawrence, Kansas 66045

S. Anderson, V. V. Frolov, Y. Kubota, S. J. Lee, R. Poling, A. Smith, C. J. Stepaniak, and J. Urheim
University of Minnesota, Minneapolis, Minnesota 55455

S. Ahmed, M. S. Alam, S. B. Athar, L. Jian, L. Ling, M. Saleem, S. Timm, and F. Wappler
State University of New York at Albany, Albany, New York 12222

(CLEO Collaboration)

We present the first measurement of the D^{*+} width using 9/fb of e^+e^- data collected near the $\Upsilon(4S)$ resonance by the CLEO II.V detector. Our method uses advanced tracking techniques and a reconstruction method that takes advantage of the small vertical size of the CESR beam spot to measure the energy release distribution from the $D^{*+} \rightarrow D^0 \pi^+$ decay. We find $\Gamma(D^{*+}) = 96 \pm 4$ (statistical) ± 22 (systematic) keV. We also measure the energy release in the decay and compute $\Delta m \equiv m_{D^{*+}} - m_{D^0} = 145.412 \pm 0.002$ (statistical) ± 0.012 (systematic) MeV/c^2.

I. INTRODUCTION

A measurement of $\Gamma(D^{*+})$ opens an important window on the nonperturbative strong physics involving heavy quarks. The basic framework of the theory is well understood, however, there is still much speculation—predictions for the width range from 15 keV to 150 keV [1]. The level splitting in the B sector is not large enough to allow real strong transitions. Therefore, a measurement of the width of the D^{*+} gives unique information about the strong coupling constant in heavy-light meson systems.

The total width of the D^{*+} is the sum of the partial widths of the strong decays $D^{*+} \rightarrow D^0 \pi^+$ and $D^{*+} \rightarrow D^+ \pi^0$ and the electromagnetic decay $D^{*+} \rightarrow D^+ \gamma$. We can write the width in terms of strong couplings, $g_{D^* \rightarrow D^0 \pi^+}$ and $g_{D^* \rightarrow D^+ \pi^0}$, and an electromagnetic coupling, $g_{D^* \rightarrow D^+ \gamma}$:

$$\Gamma(D^{*+}) = \Gamma(D^0 \pi^+) + \Gamma(D^+ \pi^0) + \Gamma(D^+ \gamma) \quad (1)$$

$$= \frac{g^2_{D^* \rightarrow D^0 \pi^+}}{24 \pi m^2_{D^{*+}}} p^3_{\pi^+} + \frac{g^2_{D^* \rightarrow D^+ \pi^0}}{24 \pi m^2_{D^{*+}}} p^3_{\pi^0}$$
$$+ \frac{\alpha g^2_{D^* \rightarrow D^+ \gamma}}{3} p^3_{\gamma}, \quad (2)$$

where the momenta are those for the indicated particle in the D^{*+} rest frame, and α is the fine structure constant. This can be rewritten using the isospin relationship

$$g_{D^* \rightarrow D\pi} = -\sqrt{2} g_{D^* \rightarrow D^+ \pi^0} = g_{D^* \rightarrow D^0 \pi^+}, \quad (3)$$

and relating $g_{D^* \rightarrow D\pi}$ to a universal strong coupling between heavy vector and pseudoscaler mesons to the pion, g, with

$$g_{D^* \rightarrow D\pi} = \frac{2m_{D^*}}{f_\pi} g, \quad (4)$$

where f_π is the pion decay constant. All this yields

---

*Permanent address: Brookhaven National Laboratory, Upton, NY 11973.

$$\Gamma(D^{*+}) = \frac{2g^2}{12\pi f_\pi^2} p_{\pi^+}^3 + \frac{g^2}{12\pi f_\pi^2} p_{\pi^0}^3 + \frac{\alpha g_{D^*\to D^+\gamma}^2}{3} p_\gamma^3.$$

(5)

The width of the D^{*+} only depends on g [2] since the contribution of the electromagnetic decay with branching fraction $(1.68\pm0.45)\%$ [3] can be neglected. The measurement of g is needed in the extraction of V_{ub} in semileptonic $b \to u$ decays [4].

Prior to this measurement, the D^{*+} width was limited to be less than 131 keV at the 90% confidence level by the ACCMOR Collaboration [5]. The limit was based on 110 signal events reconstructed in two D^0 decay channels with a background of 15%. This contribution describes a measurement of the D^{*+} width with the CLEO II.V detector where the signal, in excess of 11 000 events, is reconstructed through a single, well-measured sequence, $D^{*+} \to \pi_{slow}^+ D^0$, $D^0 \to K^- \pi^+$. Consideration of charge conjugated modes is implied throughout this paper. The level of background under the signal is less than 3% in our loosest selection.

The challenge of measuring the width of the D^{*+} is understanding the tracking system response function since the experimental resolution exceeds the width we are trying to measure. Candidates with tracks that have mismeasured hits, errors in pattern recognition, and large angle Coloumb scattering are particularly dangerous because the signal shape they project is broad and the errors for these events can be underestimated, resulting in events that can easily influence the parameters of a Breit-Wigner fitting shape. We generically term such effects "tracking mishaps." A difficulty is that there is no physical calibration for this measurement. The ideal calibration mode would have a large cross-section, a width of zero, and decay with a rather small energy release to three charged particles, one of which has a much softer momentum distribution than the other two, which decay through a nearly zero width resonance with a measurable flight distance. Such a mode would allow us to disentangle detector effects from the underlying width, but no such mode exists.

Therefore, to measure the width of the D^{*+} we depend on exhaustive comparisons between a GEANT [6] based detector simulation and our data. We addressed the problem by selecting samples of candidate D^{*+} decays using three strategies.

First we produced the largest sample from data and simulation by imposing only basic tracking consistency requirements. We call this the *nominal* sample.

Second we refine the nominal sample selecting candidates with the best measured tracks by making very tight cuts on tracking parameters. There is special emphasis on choosing those tracks that are well measured in our silicon vertex detector. This reduces our nominal sample by a factor of 30 and, according to our simulation, has negligible contribution from tracking mishaps. We call this the *tracking selected* sample.

A third alternative is to select our data on specific kinematic properties of the D^{*+} decay that minimize the dependence of the width of the D^{*+} on detector mismeasurements. The nominal sample size is reduced by a factor of 3.5 and, again according to our simulation, the effect of tracking problems is reduced to negligible levels. We call this the *kinematic selected* sample.

In all three samples the width is extracted with an unbinned maximum likelihood fit to the energy release distribution and compared with the simulation's generated value to determine a bias which is then applied to the data. These three different approaches yield consistent values for the width of the D^{*+} giving us confidence that our simulation accurately models our data.

II. CLEO DETECTOR AND DATA SAMPLES

The CLEO detector has been described in detail elsewhere. All of the data used in this analysis are taken with the detector in its II.V configuration [7]. This work mainly depends on the tracking system of the detector which consists of a three-layer, double sided silicon strip detector, an intermediate ten-layer drift chamber, and a large 51-layer helium-propane drift chamber. All three are in an axial magnetic field of 1.5 Tesla provided by a superconducting solenoid that contains the tracking region. The charged tracks are fit using a Kalman filter technique that takes into account energy loss as the tracks pass through the material of the beam pipe and detector [8].

The data were taken in symmetric e^+e^- collisions at a center of mass energy around 10 GeV with an integrated luminosity of 9.0/fb provided by the Cornell Electron-Positron Storage Ring (CESR). The nominal sample follows the selection of $D^{*+} \to \pi_{slow}^+ D^0 \to K^- \pi^+ \pi_{slow}^+$ candidates used in our D^0-$\bar{D}^0$ mixing analysis [9].

Our reconstruction method takes advantage of the small CESR beam spot and the kinematics and topology of the $D^{*+} \to \pi_{slow}^+ D^0 \to \pi_{slow}^+ K^- \pi^+$ decay chain. The K^- and π^+ are required to form a common vertex. The resultant D^0 candidate momentum vector is then projected back to the CESR luminous region to determine the D^0 production point. The CESR luminous region has a Gaussian width ~ 10 μm vertically and ~ 300 μm horizontally. It is well determined by an independent method [10]. This procedure determines an accurate D^0 production point for D^0's moving out of the horizontal plane; D^0's moving within 0.3 radians of the horizontal plane are not considered. Then the π_{slow}^+ track is refit constraining its trajectory to intersect the D^0 production point. This improves the resolution on the energy release, $Q = M(K^- \pi^+ \pi_{slow}^+) - M(K^- \pi^+) - m_{\pi^+}$, by more than 30% over simply forming the appropriate invariant masses of the tracks. The improvement to resolution is essential to our measurement of the width of the D^{*+}. Our resolution is shown in Fig. 1 and is typically 150 keV. The good agreement between Monte Carlo and data demonstrates that the kinematics and sources of uncertainties on the tracks, such as the number of hits used and the effects of multiple scattering in detector material, are well modeled.

To further improve the quality of reconstruction in our nominal sample, we apply some kinematic cuts to remove a
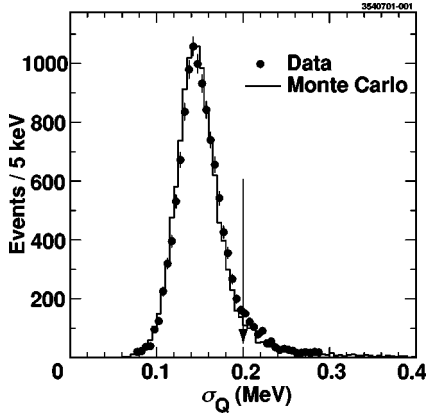
FIG. 1. Distribution of σ_Q, the uncertainty on Q as determined from propagating track fitting errors. The arrow indicates our selection to remove the long tail in the error distribution.

small amount of misreconstructed signal and background. Figure 2 shows the distribution of the momentum of the $\pi^+_{\rm slow}$ as a function of the D^{*+} candidate momentum. We apply a cut at the kinematic boundary as shown in the figure. Figure 2 also shows the opening angle θ between the $\pi^+_{\rm slow}$ and the D^0 candidate as a function of the D^{*+} candidate momentum. We apply a cut of $\theta < 38°/P_{D*}[{\rm GeV}]$ which is just beyond the kinematic limit to account for resolution smearing. We also require $\sigma_Q < 200$ keV which removes the long tail in the error distribution.

The tracking selected sample makes much more stringent cuts on the quality of the tracks used to identify the candidates. All tracks are required to have hits in both the $r\phi$ and z views in all three layers of the silicon strip detector as opposed to the nominal two silicon hits per view. None of these hits are allowed to be within 2 mm of a silicon wafer edge. The D^0 daughter tracks are required to have at least 38 of the possible 51 main drift chamber hits and seven of the ten intermediate drift chamber hits. The χ^2 per degree of freedom of the fit to these two tracks are limited to less than 2 in each of the two drift chambers and 50 in the silicon strip detector. A small fraction of candidates is uniquely removed by the last of these, 2.3% of the final sample, and its effect is negligible. These selections are designed to remove tracks that have tracking mishaps or decay in flight.

We compare the simulation and the data as a function of kinematic variables of the D^{*+} decay. This will provide an-

other test of the simulation's modeling of the data, and be the basis of our study of systematic uncertainties in the analysis. The most important kinematic variables are the "derivatives" which are defined by

$$M^2 = M(K\pi)^2 + m^2_{\pi^+_{\rm slow}} + 2(E_{D^0}E_{\pi^+_{\rm slow}} - p_{D^0}p_{\pi^+_{\rm slow}}\cos\theta),$$
(6)

$$\beta_{D^0} = p_{D^0}/E_{D^0},$$
(7)

$$\beta_{\pi^+_{\rm slow}} = p_{\pi^+_{\rm slow}}/E_{\pi^+_{\rm slow}},$$
(8)

$$\frac{\partial Q}{\partial P_{D^0}} \equiv \frac{E_{\pi^+_{\rm slow}}}{M}(\beta_{D^0} - \beta_{\pi^+_{\rm slow}}\cos\theta),$$
(9)

$$\frac{\partial Q}{\partial P_{\pi^+_{\rm slow}}} \equiv \frac{E_{D^0}}{M}(\beta_{\pi^+_{\rm slow}} - \beta_{D^0}\cos\theta),$$
(10)

$$\frac{\partial Q}{\partial \theta} \equiv \frac{p_{D^0}p_{\pi^+_{\rm slow}}}{M}\sin\theta.$$
(11)

These derivatives test correlations among the basic kinematic variables, the D^0 and $\pi^+_{\rm slow}$ momenta, and the opening angle, θ. We compare by dividing the Q distribution into ten slices in each of the kinematic variables and fitting the ten sub-distributions of Q to Gaussians. We display the width and mean of the ten fits as a function of each of the six kinematic variables in Figs. 3 and 4.

The quality of the width comparison (Fig. 3) is excellent, with the simulation generated with an underlying $\Gamma(D^{*+})$ in the range of 90–100 keV agreeing well with the data for all the kinematic variables. Even when generated with an underlying $\Gamma(D^{*+}) = 0$ keV the simulation accurately follows the data's changes as the kinematic variables vary across their allowed range.

The quality of the mean comparison (Fig. 4) is not as good. The dependence of the mean of Q is not well modeled versus the $\pi^+_{\rm slow}$ momentum, $\partial Q/\partial P_{\pi^+_{\rm slow}}$, and $\partial Q/\partial P_{D^0}$ by our simulation. We discuss the consequences of this imperfect modeling of the data in the section on systematic uncertainties below.
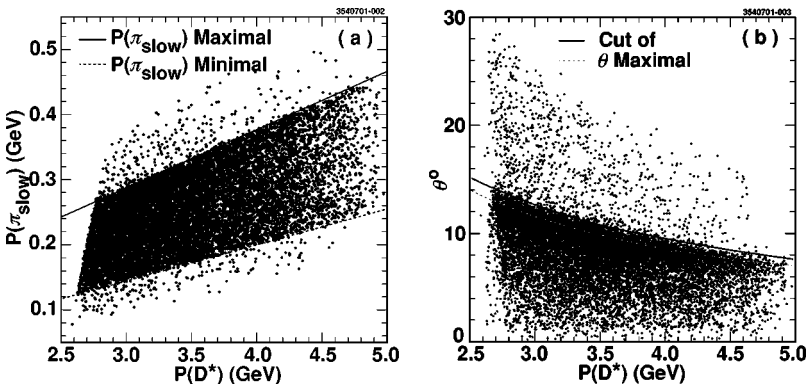

FIG. 2. The $\pi^+_{\rm slow}$ momentum (a) and the opening angle between D^0 and $\pi^+_{\rm slow}$ (b) both versus the D^{*+} momentum in the nominal data sample. In (a) the curves show kinematic boundaries where we place selections. In (b) the dotted curve shows the kinematic boundary, and the solid curve shows our selection.
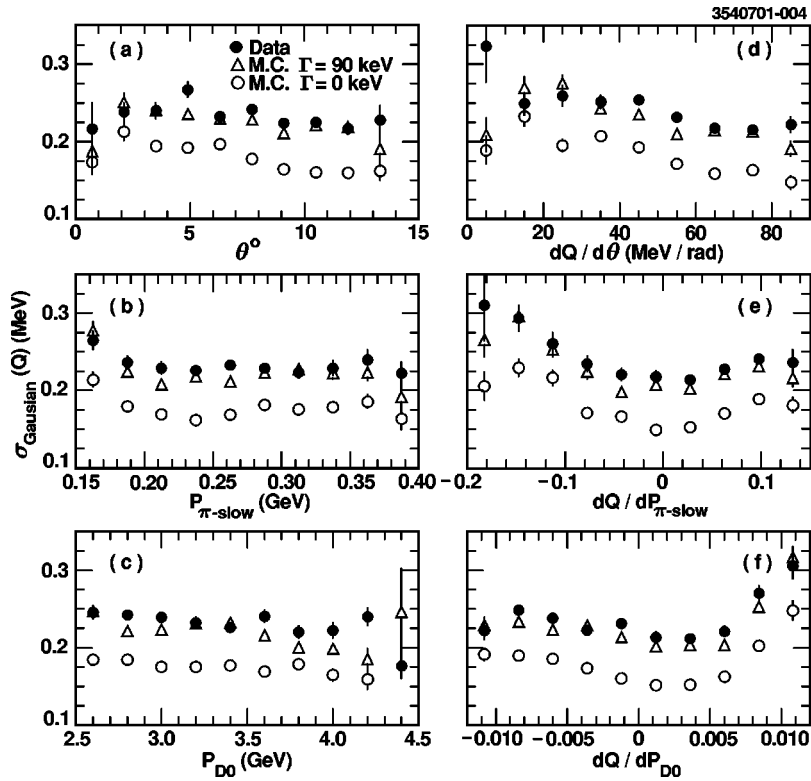
FIG. 3. Gaussian width of Q distribution versus kinematic parameters and derivatives. ●, data; ○, simulation with $\Gamma_{D^{*+}}=0$; △, simulation with $\Gamma_{D^{*+}}=90$ keV.
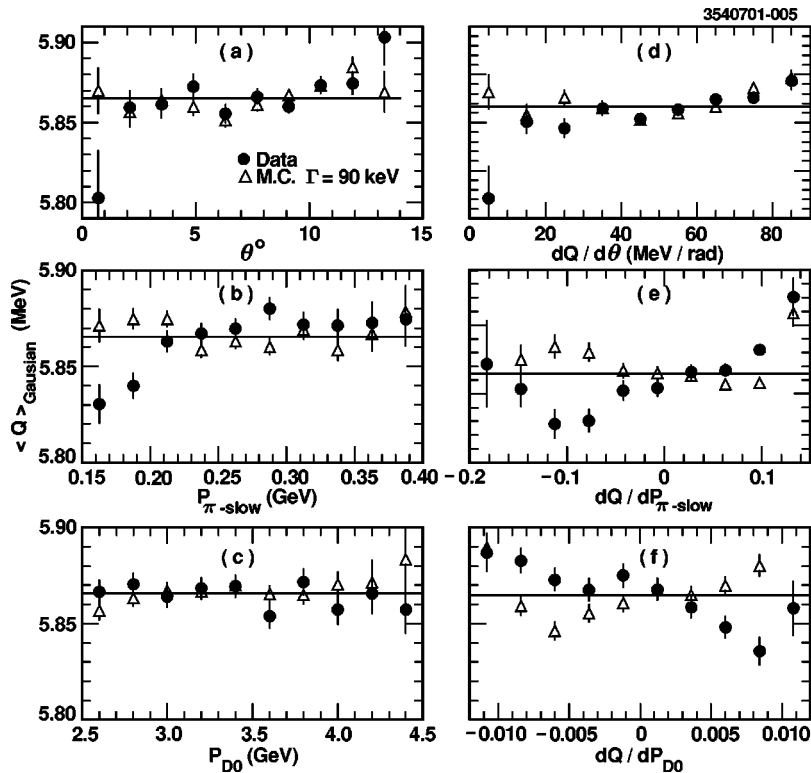

FIG. 4. Gaussian mean of Q distribution versus kinematic parameters and derivatives. ●, data; △, simulation with $\Gamma_{D^{*+}}=90$ keV. The horizontal lines show the weighted average value of Q for the two samples. These averages are made to be equal by adding a small term to the simulated sample.
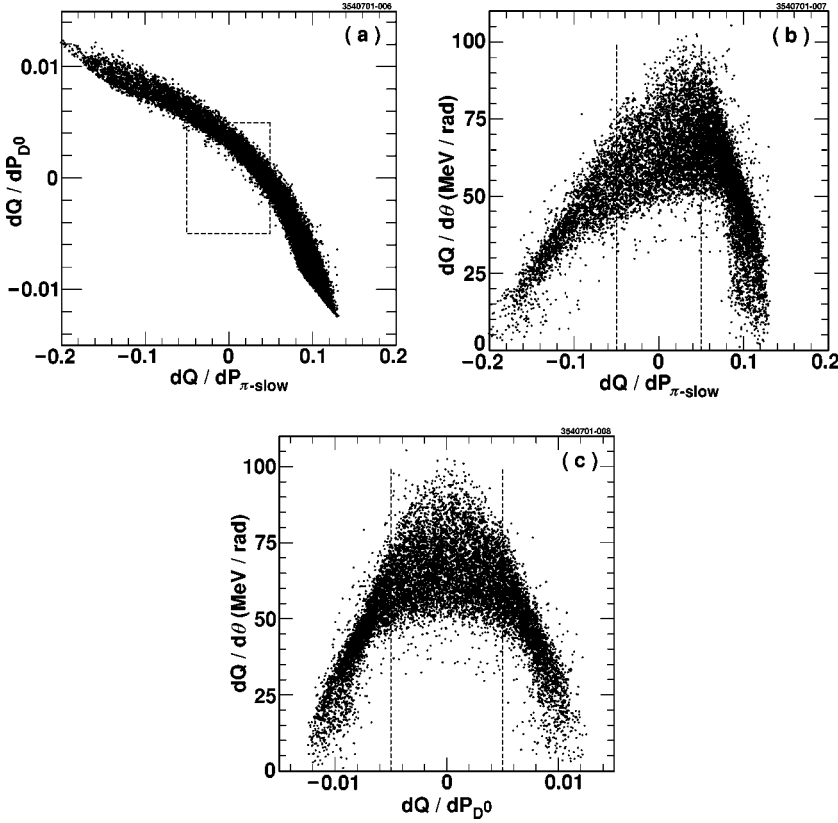
FIG. 5. Distributions of $\partial Q/\partial P_{D^0}$ versus $\partial Q/\partial P_{\pi_{slow}^+}$ (a), $\partial Q/\partial\theta$ versus $\partial Q/\partial P_{\pi_{slow}^+}$ (b), and $\partial Q/\partial\theta$ versus $\partial Q/\partial P_{D^0}$ (c) in the data. The dashed regions show the selection that defines the kinematic selected sample.

Figure 5 shows the three derivatives plotted against each other in the data. Note that if we select $\partial Q/\partial P_{D^0}$ and $\partial Q/\partial P_{\pi_{slow}^+}$ both to be close to zero we minimize the dependence of Q on the basic kinematic variables P_{D^0} and $P_{\pi_{slow}^+}$, and thus minimize the contribution of the kinematic variables to the width of the Q distribution. With this selection we are more sensitive to the underlying width of the Q distribution rather than variations caused by any mismodeling of Q's dependence on the basic kinematics. The kinematic selection is defined by

$$\left|\frac{\partial Q}{\partial P_{D^0}}\right|\leqslant 0.005, \tag{12}$$

$$\left|\frac{\partial Q}{\partial P_{\pi_{slow}^+}}\right|\leqslant 0.05. \tag{13}$$

Table IV summarizes the statistics in our three data samples. The tracking and kinematic samples are subsets of the nominal sample. The two subsets contain 94 common candidates.

III. FIT DESCRIPTION

We assume that the intrinsic width of the D^0 is negligible, $\Gamma(D^0)\ll\Gamma(D^{*+})$, implying that the width of Q is simply a convolution of the shape given by the D^{*+} width and the tracking system response function. Thus we consider the pairs of Q and σ_Q for $D^{*+}\to\pi_{slow}^+ D^0\to K^-\pi^+\pi_{slow}^+$ where
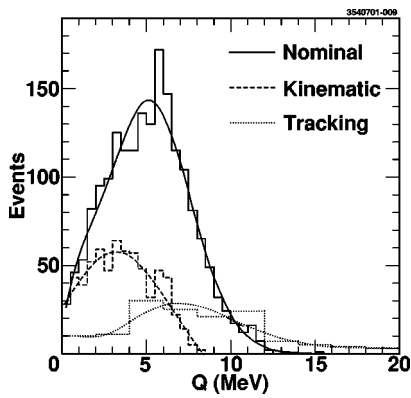

FIG. 6. Our simulation's prediction of the background for the three samples discussed in the text. Also shown are the fits to third order polynomials that are used in the fits to the data.
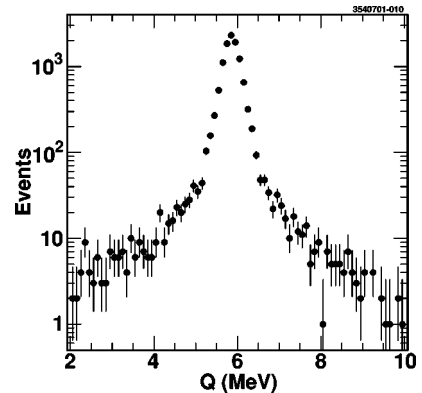

FIG. 7. The Q distribution of the nominal sample in the data.

TABLE I. Parameters of our fit to the Q distribution.

Parameter	Description
Γ_0	Breit Wigner width of Q signal distribution, $\Gamma(D^{*+})$
Q_0	Mean of Q signal distribution
N_s	Number of signal events
f_{mis}	Fraction of mismeasured signal
σ_{mis}	Resolution on measured Q for mismeasured signal
N_b	Number of background events
k	σ_Q scale factor, fixed to 1
$B_{1,2,3}$	Coefficients of background polynomial, fixed from simulation

σ_Q is given for each candidate by propagating the tracking errors in the kinematic fit of the charged tracks. We perform an unbinned maximum likelihood fit to the Q distribution.

The underlying signal shape of the Q distribution is assumed to be given by a P-wave Breit-Wigner with central value of Q, Q_0. We considered a relativistic and non-relativistic Breit-Wigner as a model of the underlying signal shape, and found negligible changes in the fit parameters between the two. The width of the signal Breit-Wigner depends on Q and is given by

$$\Gamma(Q) = \Gamma_0 \left(\frac{P}{P_0}\right)^3 \left(\frac{M_0}{M}\right)^2, \tag{14}$$

where Γ_0 is equivalent to $\Gamma(D^{*+})$, P and M are the candidate π^+_{slow} or D^0 momentum in the D^{*+} rest frame and $K\pi\pi_{\text{slow}}$ mass, and P_0 and M_0 are the values computed using Q_0. The effect of the mass term is negligible at our energy. The partial width and the total width differ negligibly in their dependence on Q for $Q > 1$ MeV.

For each candidate the signal shape is convolved with a resolution Gaussian with width σ_Q, determined by the tracking errors, as a model of our finite resolution shown in Fig. 1.

The fit also includes a background contribution with a fixed shape. The shape for the background is taken from fits to the background prediction of our simulation with a third order polynomial. The level of the background is allowed to float in our standard fit. The predicted background shape and fits are displayed in Fig. 6.

Figure 7 shows the Q distribution for our nominal data sample. Note that besides the well measured signal and the small, slowly varying background, there is also a small component centered on the signal with a large width. Therefore we allow a small fraction of the signal, f_{mis}, to be parametrized by a single Gaussian resolution function of width σ_{mis}. This shape is included in the fit to model the tracking mishaps which our simulation predicts to be at the 5% level in the nominal sample and negligible in both the tracking and kinematic selected samples. Typically we constrain the level of this contribution while allowing σ_{mis} to float.

We have many other parameters of the fit that can be varied or allowed to float for testing purposes. We can allow a scale factor on each candidate's σ_Q to model a systematic mistake in our tracking system caused, for example, by not properly accounting for the material of the detector. In our standard fits we only allow the normalization of the background to float, but we can either vary the shape as indicated by the simulation or allow the parameters of the background polynomial to float as a measure of the small systematic uncertainty due to the background shape.

Table I summarizes the parameters of our fit. Note that the σ_Q scale factor k and the background shape parameters $B_{1,2,3}$ are fixed in our nominal fits. We minimize the likelihood function

$$L = 2(N_s + N_b)$$
$$- 2 \sum_{i=1}^{N} \log[N_s S(Q_i, \sigma_{Qi}; \Gamma_0, Q_0, f_{mis}, \sigma_{mis}, k)$$
$$+ N_b B(Q_i; B_{1,2,3})], \tag{15}$$

TABLE II. Summary of fits to the simulated samples.

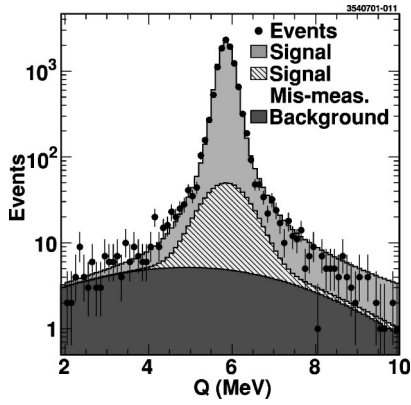| $\Gamma_{\text{generated}}$ (keV)	$\Gamma_{\text{fit}} - \Gamma_{\text{generated}}$ (keV) in sample		
	Nominal	Tracking	Kinematic
70	2.2 ± 5.0	-6.0 ± 12.4	11.7 ± 7.1
80	2.7 ± 5.2	-5.2 ± 14.2	3.9 ± 7.4
90	7.2 ± 5.7	33.5 ± 21.4	19.5 ± 8.8
100	-2.2 ± 5.4	4.1 ± 18.2	-6.3 ± 7.8
110	-2.7 ± 5.7	-9.2 ± 18.8	-5.4 ± 8.3
120	7.1 ± 6.1	18.2 ± 21.5	7.7 ± 9.3
130	6.9 ± 6.4	2.8 ± 18.7	-1.0 ± 9.4

FIG. 8. Fit to nominal data sample. The different contributions to the fit are shown by different colors or patterns.

where S and B are respectively the signal and background shapes discussed above.

The fitter has been extensively tested both numerically and with input from our full simulation. We find that the fitter performs reliably giving normal distributions for the floating parameters and their uncertainties. It also reproduces the input $\Gamma(D^{*+})$ from 0 to 130 keV. Its behavior on each of the three data samples—nominal, tracking selected, and kinematic selected—in the full simulation is discussed below. We note that if all the parameters are allowed to vary simultaneously there is strong correlation among the intrinsic width, Γ_0, the fraction of mismeasured events, f_{mis}, and the σ_Q scale factor, k, as one would expect. Thus our nominal fit holds k fixed, but in our systematic studies we either fix one of the three or provide a constraint with a contribution to the likelihood if the parameter varies from its nominal value.

IV. FIT RESULTS

As a preliminary test to fitting the data we run the complete analysis on a fully simulated sample that has about ten times the data statistics and is generated with a range of underlying $\Gamma(D^{*+})$ from 0 to 130 keV. We do this for nominal, tracking, and kinematic selected samples. For the nominal sample we note that the fit is not stable if all the param-
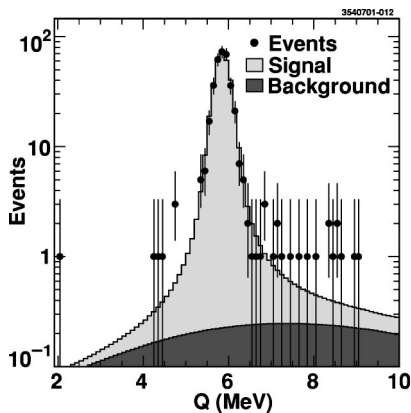
eters are left to vary freely. We have found that if we constrain the fraction of mismeasured signal to $(5.3\pm0.5)\%$ as indicated by the simulation over the range of generated widths of the D^{*+} then we get a stable result. This constraint makes the fit to the simulated nominal sample have no significant offset between the generated and measured values for the width of the D^{*+}. The tracking and kinematic selected samples have a negligible amount of mismeasured signal according to the simulation and in fits to these samples we fix f_{mis} to zero. These simulated samples are also consistent with no offset between the generated and measured values for the width of the D^{*+}. We also note that in all three simulated samples there are no trends in the difference between measured and generated width as a function of the generated width; the offset is consistent with zero as a function of the generated width of the D^{*+}. Table II summarizes this simulation study and the weighted average offsets are given in Table IV. We will apply these offsets to the fit value that we obtain from the data. For the energy release all samples show small shifts, -7 ± 3 keV for the nominal, -12 ± 10 keV for the tracking, and -12 ± 5 keV for the kinematic. Note that the errors on these offsets are accounted for as systematic uncertainties in Sec. V.

Figures 8, 9, and 10 respectively display the fit to the nominal, tracking, and kinematic selected data samples. The results of the fits are summarized in Table III. Correlations among the floating parameters of the fit are negligible. Figure 11 displays the likelihood as a function of the width of the D^{*+} for the fits to the three data samples.

The agreement is excellent among the three fits, and when the offsets from Table IV are applied we obtain

$$\text{nominal sample } \Gamma(D^{*+})=96.2\pm4.0 \text{ keV}, \quad (16)$$

$$\text{tracking selected } \Gamma(D^{*+})=104\pm20 \text{ keV}, \quad (17)$$

$$\text{kinematic selected } \Gamma(D^{*+})=103.8\pm5.9 \text{ keV}. \quad (18)$$

The results on the width to the three samples in the data are summarized in Table IV. The uncertainties are only statistical. We discuss systematic uncertainties in the next section.

FIG. 9. Fit to tracking selected data sample. The different contributions to the fit are shown by different colors or patterns.
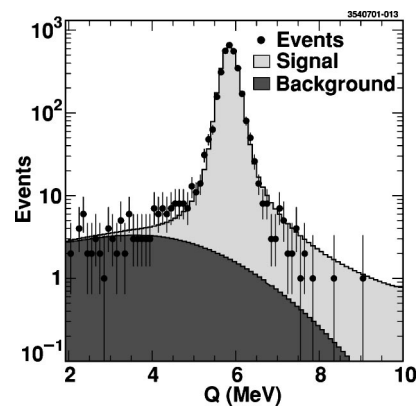

FIG. 10. Fit to kinematic selected data sample. The different contributions to the fit are shown by different colors or patterns.
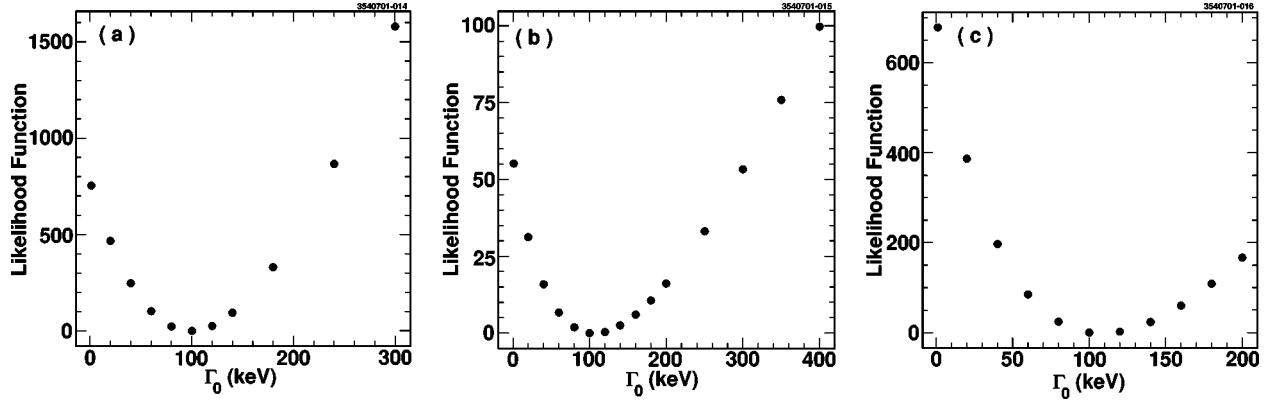
FIG. 11. Likelihood function versus measured D^{*+} width for the nominal (a), tracking (b), and kinematic (c) selected data samples.

V. SYSTEMATIC UNCERTAINTIES

We discuss the sources of systematic uncertainties on our measurements of the width of the D^{*+} in the order of their size. The most important contribution is the variation of the results as a function of the kinematic parameters of the D^{*+} decay as shown most clearly in Fig. 4. We estimate this uncertainty by repeating the fits described above in three bins for each of the six kinematic parameters and taking the uncertainty as the largest observed variation from the nominal values in Table III. We obtain uncertainties of ± 16 and ± 8 keV on $\Gamma(D^{*+})$ and Q_0 respectively.

The next most important contribution comes from any mismodeling of σ_Q's dependence on the kinematic parameters. We estimate this by varying our cut on σ_Q from 75 to 400 from the nominal 200 keV and repeating our analysis with all parameters fixed except allowing the error scale factor k to vary freely. This indicates that the resolution is correct to $\pm 4\%$, and we then repeat our standard analysis with k fixed at 0.96 and 1.04. We find uncertainties of ± 11, ± 9, and ± 7 keV on $\Gamma(D^{*+})$ for the nominal, tracking, and kinematic selected sample. For Q_0 this uncertainty is negligible except in the tracking selected sample where it is ± 4 keV.

We take into account correlations among the less well measured parameters of the fit, such as k, f_{mis}, and σ_{mis}, by fixing each parameter at $\pm 1\sigma$ from their central fit values, repeating the fit, and adding in quadrature the variation in the width of the D^{*+} and Q_0 from their central values. We find uncertainties of ± 8, ± 9, and ± 9 keV on the width of

the D^{*+} for the nominal, tracking, and kinematic selected sample, and respectively ± 3, ± 4, and ± 5 keV on Q_0.

We have studied in the simulation the sources of mismeasurement that give rise to the resolution on the width of the D^{*+} by replacing the measured values with the generated values for various kinematic parameters of the decay products. We have then compared these uncertainties with analytic expressions for the uncertainties. The only source of resolution that we cannot account for in this way is a small distortion of the kinematics of the event caused by the algorithm used to reconstruct the D^0 origin point described above. This contributes an uncertainty ± 4 keV on the width of the D^{*+} and ± 2 keV on Q_0. We have also checked that our simulation accurately models the line shape of other narrow resonances visible in our data. Notably the decay $\Lambda^0 \rightarrow p \pi^-$ has a Q only seven times that of $D^{*+} \rightarrow D^0 \pi^+_{\text{slow}}$. In the Λ^0 decay we select the π^- to have a momentum in the range of those in the D^{*+} decay, and the visible widths agree to a few percent between data and simulation.

We consider uncertainties from the background shape by allowing the coefficients of the background polynomial to float. We observe changes on the width of ± 4 keV for the nominal sample and ± 2 keV for the tracking and kinematic selected samples. We have also released our kinematic selection cuts, which causes the background to increase by a large factor. This causes a change which is small compared to allowing the coefficients of the background shape polynomial to float. Variations in the background have a negligible effect on Q_0.

TABLE III. Results for the parameters of the fit to the three data samples. The fit parameters are summarized in Table I. The uncertainties are statistical.

Parameter		Sample	
	Nominal	Tracking	Kinematic
Γ_0 (keV)	98.9 ± 4.0	106.0 ± 19.6	108.1 ± 5.9
Q_0 (keV)	5853 ± 2	5854 ± 10	5850 ± 4
N_s	11207 ± 109	353 ± 20	3151 ± 57
f_{mis} (%)	5.3 ± 0.5	NA	NA
σ_{mis} (keV)	508 ± 39	NA	NA
N_b	289 ± 31	15 ± 7	133 ± 16

TABLE IV. Summary of the data sample, simulation biases, and fit results. The error on the D^{*+} width is only statistical.

Parameter	Nominal	Sample Tracking	Kinematic
Candidates	11496	368	3284
Background fraction (%)	2.51±0.27	4.1±1.9	4.05±0.49
$\Gamma_{fit} - \Gamma_{generated}$ (keV)	2.7±2.1	1.7±6.4	4.3±3.1
Fit Γ_0 (keV)	98.9±4.0	106.0±19.6	108.1±5.9
D^{*+} width (keV)	96.2±4.0	104±20	103.8±5.9

Minor sources of uncertainty are from the width offsets derived from our simulation and given in Table IV, and our digitized data storage format which saves track parameters with a resolution of 1 keV and contributes an uncertainty of ± 1 keV on the width of the D^{*+} and Q_0.

An extra and dominant source of uncertainty on Q_0 is the energy scale of our measurements. We evaluate this uncertainty by selecting $K_s \rightarrow \pi^+\pi^-$ decays in our data. The daughters tracks of the K_s candidates are required to pass the same selection criterion as those described above in the nominal sample, the decay vertex is required to be inside the beam pipe, and the vertex is required to be significantly separated from the overall event vertex. Our K_s sample is quite clean, less than 1% background under the mass peak, and has millions of candidates. We then plot the mean of the $\pi^+\pi^-$ invariant mass as a function of the momentum of the daughters. We find that above a daughter momentum of 500 MeV/c the K_s mass agrees with its expected value [11]. We apply corrections, less than 0.3% relative, to tracks between 100 and 500 MeV/c to bring the mass peaks into agreement with the nominal value. These corrections only affect the slow pion and produce a shift in Q_0 of -4 keV and a negligible change in the width. We evaluate uncertainties in the energy scale by varying an overall momentum scale to give a ± 30 keV variation, the uncertainty, of the $K_s \rightarrow \pi^+\pi^-$ mass, and applying the statistical errors we obtain from the calculations of the momentum corrections discussed above. Conservatively we add in quadrature twice the observed shift. We observe an uncertainty of 8 keV on Q_0

and 1 keV on the width due to uncertainty in the energy scale of our measurements.

Table V summarizes the systematic uncertainties on the width of the D^{*+} and Q_0.

VI. CONCLUSION

We have measured the width of the D^{*+} by studying the distribution of the energy release in $D^{*+} \rightarrow D^0 \pi^+$ followed by $D^0 \rightarrow K^-\pi^+$ decay. We have done this in three separate samples, one that is minimally selected, a second that reduces poorly measured tracks due to misassociated hits and non-Gaussian multiple scattering in the detector material, and a third that takes advantage of the kinematics of the decay chain to reduce dependence on mismeasurements of kinematic parameters. The resolution on the energy release is well modeled by our simulation, with agreement between the sources of the resolution as predicted by the simulation and analytic calculations. The largest sources of uncertainty are imperfect modeling of the dependence of the mean energy release on the kinematics of the decay chain, the simulation of the error on the energy release, and correlations among the parameters of the fit to the energy release distribution. With our estimate of the systematic uncertainties for each of the three samples being essentially the same we chose to report the result for the sample with the smallest statistical uncertainty, the minimally selected sample, and obtain

$$\Gamma(D^{*+}) = 96 \pm 4 \pm 22 \text{ keV}, \qquad (19)$$

TABLE V. Systematic uncertainties on the width of the D^{*+} and Q_0.

Source	Nominal $\delta\Gamma(D^{*+})$	Nominal δQ_0	Sample Tracking $\delta\Gamma(D^{*+})$	Sample Tracking δQ_0	Kinematic $\delta\Gamma(D^{*+})$	Kinematic δQ_0
Dependence on kinematics	16	8	16	8	16	8
Mismodeling of σ_Q	11	<1	9	4	7	<1
Fit correlations	8	3	9	4	9	5
Vertex reconstruction	4	2	4	2	4	2
Background shape	4	<1	2	<1	2	<1
Offset correction	2	3	6	10	3	5
Energy scale	1	8	1	8	1	8
Data digitization	1	1	1	1	1	1
Quadratic sum	22	12	22	16	20	14

where the first uncertainty is statistical and the second is systematic. We note that if we form an average value taking into account the statistical correlations among our three measures we get a result that is nearly identical with Eq. (19) since the average is dominated by the result with the smallest statistical uncertainty.

This is the first measurement of the width of the D^{*+}, and our measurement corresponds to a strong coupling [1]

$$g = 0.59 \pm 0.01 \pm 0.07, \tag{20}$$

and

$$g_{D^* \to D\pi} = 17.9 \pm 0.3 \pm 1.9. \tag{21}$$

This is consistent with theoretical predictions based on heavy quark effective theory (HQET) and relativistic quark models, but higher than predictions based on QCD sum rules.

We also measure the mean value for the energy release in $D^{*+} \to D^0 \pi^+$ decay

$$Q_0 = 5842 \pm 2 \pm 12 \text{ keV}, \tag{22}$$

where the first error is statistical and the second is systematic. Combining this with the mass of the charged pion, 139.570 MeV, with an uncertainty less than 1 keV [11], we calculate

$$m_{D*(2010)^+} - m_{D^0} = 145.412 \pm 0.002 \pm 0.012 \text{ MeV}. \tag{23}$$

This agrees with the value from the Particle Data Group, 145.436 ± 0.016 MeV, from a global fit of all flavors of D^*–D mass differences. It also agrees well with the best previous measure from a single experiment that includes an evaluation of systematic uncertainties from ACCMOR at 145.39 ± 0.07 MeV [5].

[1] V. M. Belyaev *et al.*, Phys. Rev. D **51**, 6177 (1995) contains a recent survey summarizing and referencing previous theoretical work. P. Singer, Acta Phys. Pol. B **30**, 3849 (1999); J. L. Goity and W. Roberts, Phys. Rev. D **64**, 094007 (2001); K. O. E. Henriksson *et al.*, Nucl. Phys. **A686**, 355 (2001); M. Di Pierro and E. Eichten, Phys. Rev. D **64**, 114004 (2001) have appeared since that survey.

[2] M. Wise, Phys. Rev. D **45**, R2188 (1992); G. Burdman and J. F. Donoghue, Phys. Lett. B **280**, 287 (1992); T. Yan *et al.*, Phys. Rev. D **46**, 1148 (1992); **55**, 5851(E) (1997); D. Becirevic and A. L. Yaouanc, J. High Energy Phys. **03**, 021 (1999), contains a recent review referencing previous theoretical work.

[3] CLEO Collaboration, J. Bartelt *et al.*, Phys. Rev. Lett. **80**, 3919 (1998).

[4] G. Burdman, Z. Ligeti, M. Neubert, and Y. Nir, Phys. Rev. D **49**, 2331 (1994).

[5] S. Barlag *et al.*, Phys. Lett. B **278**, 480 (1992).

[6] R. Brun *et al.*, GEANT3 Users Guide, CERN DD/EE/84-1.

[7] CLEO Collaboration, Y. Kubota *et al.*, Nucl. Instrum. Methods Phys. Res. A **320**, 66 (1992); T. Hill, *ibid.* **418**, 32 (1998).

[8] P. Billior, Nucl. Instrum. Methods Phys. Res. A **225**, 352 (1984).

[9] CLEO Collaboration, R. Godang *et al.*, Phys. Rev. Lett. **84**, 5038 (2000).

[10] D. Cinabro *et al.*, CLNS 00/1706, physics/0011075.

[11] Particle Data Group, D. E. Groom *et al.*, Eur. Phys. J. C **15**, 1 (2000).